The PqsE active site as a target for small molecule antimicrobial agents against *Pseudomonas aeruginosa*

Isabelle R. Taylor[1], Philip D. Jeffrey[1], Dina A. Moustafa[2], Joanna B. Goldberg[2], Bonnie L. Bassler[1,3*]

[1]Department of Molecular Biology, Princeton University, Princeton, NJ 08544, USA.

[2]Emory University School of Medicine, Children's Healthcare of Atlanta, Inc., Department of Pediatrics, and Center for Cystic Fibrosis and Airway Diseases Research, Atlanta, GA 30322, USA.

[3]Howard Hughes Medical Institute, Chevy Chase, MD 20815, USA.

*To whom correspondence should be addressed. Email: bbassler@princeton.edu

Key Words: *Pseudomonas aeruginosa*, quorum sensing, antibiotics, protein-protein interactions, allosteric inhibitors

Abstract

The opportunistic pathogen *Pseudomonas aeruginosa* causes antibiotic resistant, nosocomial infections in immuno-compromised individuals, and is a high priority for antimicrobial development. Key to pathogenicity in *P. aeruginosa* are biofilm formation and virulence factor production. Both traits are controlled by the cell-to-cell communication process called quorum sensing (QS). QS involves the synthesis, release, and population-wide detection of signal molecules called autoinducers. We previously reported that activity of the RhlR QS transcription factor depends on a protein-protein interaction with the hydrolase, PqsE, and PqsE catalytic activity is dispensable for this interaction. Nonetheless, the PqsE-RhlR interaction could be disrupted by substitution of an active site glutamate residue with tryptophan (PqsE(E182W)). Here, we show that disruption of the PqsE-RhlR interaction via either the E182W change or alteration of PqsE surface residues that are essential for the interaction with RhlR, attenuates *P. aeruginosa* infection in a murine host. We use crystallography to characterize the conformational changes induced by the PqsE(E182W) substitution to define the mechanism underlying disruption of the PqsE-RhlR interaction. A loop rearrangement that repositions the E280 residue in PqsE(E182W) is responsible for the loss of interaction. We verify the implications garnered from the PqsE(E182W) structure using mutagenic, biochemical, and additional structural analyses. We present the next generation of molecules targeting the PqsE active site, including a structure of the tightest binding of these compounds, BB584, in complex with PqsE. The findings presented here provide insight for drug discovery against *P. aeruginosa* with PqsE as the target.

42

43 **Author Summary**

44

45 The human pathogen *Pseudomonas aeruginosa* is resistant to many currently used
46 antibiotics, making it a burden of urgent clinical importance. *P. aeruginosa* pathogenicity
47 is controlled by the bacterial cell-to-cell communication process called quorum sensing
48 (QS). The function of one protein that controls *P. aeruginosa* QS-directed virulence, RhlR,
49 requires a protein-protein interaction with an enzyme called PqsE. When PqsE is blocked
50 from interacting with RhlR, *P. aeruginosa* is avirulent and incapable of infecting an animal
51 host. Here, we validate the PqsE-RhlR interaction as a target for antibiotic development,
52 and we present a mechanism for how such antibiotics could disrupt the PqsE-RhlR
53 interaction. Discovery of new antibiotics would fulfill an unmet healthcare need by
54 providing treatments to combat *P. aeruginosa* infections.

55

56 **Introduction**

57

58 *Pseudomonas aeruginosa* is an opportunistic human pathogen that is responsible
59 for untreatable infections in vulnerable, immuno-compromised individuals (1,2). As a
60 member of the "ESKAPE" multi-drug resistant pathogens, *P. aeruginosa* is a high-priority
61 target for the development of next generation antibiotics that function by new mechanisms
62 of action (3,4). Features contributing to *P. aeruginosa* pathogenicity include the ability to
63 produce virulence factors and form biofilms (5). These traits are controlled by the bacterial
64 cell-cell communication process called quorum sensing (QS) (6,7).

65 QS involves the production, release, and population-wide detection and response
66 to signal molecules called autoinducers (8). *P. aeruginosa* QS relies on two acyl-
67 homoserine lactone (HSL) autoinducer production/detection systems, called Las and Rhl,
68 and the Pqs alkyl quinolone autoinducer production/detection system (9–11). The Las
69 system consists of the LasI autoinducer synthase and LasR receptor/transcription factor
70 which, respectively, produce and detect the autoinducer 3-oxo-C12-HSL (12). The Rhl
71 system consists of the RhlI autoinducer synthase and the RhlR receptor/transcription
72 factor, which, respectively, produce and detect the autoinducer C4-HSL (13) (Figure 1a).
73 The Pqs system consists of the PQS autoinducer, synthesized by PqsABCD, and its
74 partner receptor/transcription factor, PqsR (14,15). The Las system sits at the top of the
75 *P. aeruginosa* QS hierarchy and controls transcription of the components of the Rhl and
76 Pqs systems (16). Curiously, RhlR function additionally depends on the metallo-β-
77 hydrolase enzyme PqsE, encoded as the final gene in the *pqsABCDE* biosynthetic operon
78 (17–19). With respect to RhlR, PqsE is required to form a protein-protein interaction that
79 enhances the affinity of RhlR for target promoters (20,21). Moreover, the RhlR-PqsE
80 interaction is essential for *P. aeruginosa* virulence phenotypes, and therefore, of interest
81 as a focus for antibiotic development.

82 We recently showed that the ability of PqsE to interact with RhlR can be weakened
83 by introduction of an “inhibitor mimetic” mutation in which the glutamate residue at
84 position 182 is altered to tryptophan (PqsE(E182W)) (20). The PqsE(E182W) variant is a
85 stable protein that, while harboring all of the catalytic residues, nonetheless displays less
86 than 10% of wildtype catalytic activity, as if an inhibitor is bound in the active site. Residue
87 E182 is buried deep within the active site of PqsE, at a location distant from the three

88 surface arginine residues (R243, R246, and R247) that are necessary for PqsE to interact
89 with RhlR. Mutation of the PqsE R243, R246, and R247 residues to alanine completely
90 abolishes the PqsE-RhlR interaction (21). When introduced into *P. aeruginosa*, neither
91 PqsE(E182W) nor PqsE(R243A/R246A/R247A) (the latter called PqsE(NI) for "non-
92 interacting"), can promote PqsE-RhlR-dependent virulence phenotypes, including
93 production of the pyocyanin toxin. The effects of the PqsE E182W and PqsE NI
94 substitutions on pyocyanin production are not through impairment of PqsE catalytic
95 function, as the catalytically inactive variant, PqsE(D73A), remains fully capable of
96 interacting with RhlR and driving pyocyanin production. These results indicate that PqsE
97 has two independent functions, catalysis and interaction with RhlR, and it is interaction
98 with RhlR, not catalysis, that is required for virulence.

99 From a drug discovery perspective, it is particularly promising that the PqsE active
100 site E182W mutation weakens the distal PqsE-RhlR interaction, the consequence of
101 which is suppression of virulence phenotypes. We assert this because a PqsE active site-
102 targeting molecule would likely be able to bind with high affinity and be more amenable
103 to medicinal chemistry than a molecule targeting the interaction site on the surface of the
104 protein. Protein-protein interactions, which typically occur over large, shallow protein
105 surfaces, have proven notoriously difficult to target with small molecules (22). Molecules
106 that can bind in protein-protein interaction domains typically do so with weak affinity, are
107 large and structurally complicated, and are difficult to optimize through medicinal
108 chemistry efforts (23). With this notion in mind, in this study, we aimed to determine the
109 mechanism by which the PqsE E182W mutation disrupts the PqsE-RhlR interaction, and
110 whether it is possible to achieve a similar effect with a small molecule inhibitor that binds

111 in the PqsE active site. In a proof of principle experiment, we use our PqsE variants to
112 demonstrate that disrupting the PqsE-RhlR interaction indeed attenuates *in vivo P.*
113 *aeruginosa* virulence in a mouse lung infection model. We employ crystallography to
114 characterize the structure of the PqsE(E182W) protein. We probe the functions of the
115 PqsE active site through mutagenesis. Finally, we present the next generation of PqsE
116 active site-targeting small molecules for further synthetic optimization. Our results can
117 inform the discovery and/or design of effective antimicrobial agents to treat *P. aeruginosa*
118 infections.
119
120 **Results**
121
122 *PqsE variants that cannot interact with RhlR display attenuated infection phenotypes in*
123 *cell assays and in a mouse lung infection model.*
124 We have shown previously that, unlike overexpression of wildtype (WT) *pqsE*,
125 overexpression of *pqsE* mutants encoding proteins that cannot interact with RhlR *in vitro*
126 are impaired in promoting pyocyanin production in Δ*pqsE P. aeruginosa* PA14 (20,21).
127 To verify that the PqsE variants of interest display similar defects in virulence phenotypes
128 when the genes encoding them are expressed from the native locus, we constructed *P.*
129 *aeruginosa* PA14 strains harboring *pqsE(D73A)*, *pqsE(E182W)*, and *pqsE(NI)* on the
130 chromosome. Western blots showed that the WT and variant PqsE proteins were
131 produced at the same levels and exhibited similar stabilities (Figure S1). WT *P.*
132 *aeruginosa* PA14 made pyocyanin while the Δ*pqsE* strain did not (4% compared to WT).
133 When the PqsE variant proteins were produced from the chromosomally-encoded genes,

134 the results were entirely consistent with our previous findings for each PqsE variant
135 produced from a plasmid. Specifically, the catalytically inactive PqsE(D73A) variant made
136 nearly WT levels of pyocyanin (96%), the PqsE(E182W) inhibitor mimetic variant was
137 severely impaired (17%), and the PqsE(NI) variant was incapable of driving pyocyanin
138 production (4%) (Figure 1b).

139 Previously, we showed that the *P. aeruginosa* PA14 Δ*rhlI* strain forms smooth
140 colonies whereas the Δ*rhlI* Δ*rhlR* and Δ*rhlI* Δ*pqsE* double mutants form biofilms with
141 hyper-rugose morphologies (24,25). Thus, both PqsE and RhlR are required to suppress
142 hyper-rugose biofilm formation in the absence of the C4-HSL autoinducer. To determine
143 which specific function of PqsE, catalysis and/or interaction with RhlR, is linked to the
144 control of biofilm morphology, we tested our PqsE variants. Each *pqsE* mutant was
145 incorporated at the native chromosomal locus in the Δ*rhlI* strain and biofilm morphology
146 was assessed (Figure 1c). Both the Δ*rhlI pqsE(E182W)* and Δ*rhlI pqsE(NI)* mutants
147 formed hyper-rugose biofilms similar to those of the Δ*rhlI* Δ*rhlR* and Δ*rhlI* Δ*pqsE* mutants.
148 Only the Δ*rhlI* strain harboring the *pqsE(D73A)* mutation exhibited the smooth biofilm
149 morphology of the parent Δ*rhlI* strain. This result demonstrates that the PqsE-RhlR
150 interaction controls biofilm morphology, and that PqsE catalytic activity is dispensable for
151 this trait.

152 To explore the individual roles of PqsE catalysis and PqsE-RhlR interaction during
153 host infection, we assessed the relative pathogenicity of WT *P. aeruginosa* PA14, Δ*pqsE*,
154 *pqsE(D73A)*, *pqsE(E182W)*, and the *pqsE(NI)* strains in a murine model of acute
155 pneumonia. Mice were infected intratracheally with equal strain inoculum levels (~$3x10^6$
156 CFU/mouse) and monitored over 48 h of infection. At 24 h, mice from all infection groups

157 exhibited mild to moderate symptoms in response to infection, primarily displaying
158 decreased mobility and increased breathing. Consistent with these symptoms,
159 comparable levels of lung colonization were observed among all groups (Figure 1d). At
160 48 h, however, mice infected with either WT *P. aeruginosa* PA14 or the *pqsE(D73A)*
161 mutant became more lethargic and appeared to progressively manifest additional
162 symptoms, including increasingly labored breathing, hunched posture, and decreased
163 response to stimuli. Moreover, those mice demonstrated >2 log increase in the bacterial
164 burden compared to 24 h. In stark contrast, mice infected with the Δ*pqsE*, *pqsE(E182W)*,
165 or *pqsE(NI)* strains continued to display mild clinical symptoms with almost no change in
166 their lung bacterial burden (Figure 1d). Together, the above findings demonstrate that
167 the PqsE-RhlR interaction, and not PqsE catalytic activity, is responsible for shaping the
168 pathogenicity of *P. aeruginosa* PA14 *in vitro* and *in vivo*.
169
170 *The PqsE E182W substitution induces a loop rearrangement near the active site.*
171 The above murine infection experiment demonstrated that weakening the ability of
172 PqsE to interact with RhlR by mutating an active site residue (PqsE(E182W)) causes a
173 similarly severe reduction in infectivity to that caused by complete elimination of the PqsE-
174 RhlR interaction (PqsE(NI)). To understand, at an atomic level, what conformational
175 changes the E182W alteration induced in PqsE to affect its ability to interact with RhlR,
176 we determined the structure of PqsE(E182W) (Figure 2a). Although the PqsE(E182W)
177 crystals grow in the same $P3_221$ crystal form as WT PqsE, there is significant structural
178 rearrangement in the active site. In WT PqsE, the sidechain of E182 lies at the edge of
179 the ligand binding site and makes hydrogen bonds with R191 and Q272. These

180 interactions do not occur in PqsE(E182W), and rather, new interactions are made
181 between the sidechain of the introduced W182 residue and F276, L277, and P278. The
182 E182W change induces the rearrangement of the G270-L281 loop between helices 6 and
183 7, with a portion of that loop becoming disordered. Examination of electron density within
184 the active site indicated a surprising consequence - with the sidechain of E280 relocating
185 by 12 Å and becoming Fe bound in the center of the active site. Indeed, the repositioned
186 E280 sidechain directly binds both Fe atoms, acting as a bridging ligand, and thus is most
187 likely responsible for the stabilizing effect the E182W alteration has on PqsE, which we
188 have reported previously (20).

189 To test whether repositioning of PqsE residue E280 underpinned the inhibitor
190 mimetic characteristics of the PqsE(E182W) protein, we engineered the E280A
191 substitution into PqsE(E182W) to make PqsE(E182W/E280A). We determined the crystal
192 structure of PqsE(E182W/E280A) revealing further changes in the PqsE active site. In
193 this case, the presence of an alanine at residue 280 eliminated interaction with the iron
194 atoms, and the loop consisting of residues D275-L281 was disordered (Figure 2b). The
195 remainder of the loop was ordered and its structure reverted to a conformation that was
196 more native-like than in PqsE(E182W). Consequently, the removal of the glutamate-Fe
197 interaction via the E280A substitution apparently unblocked the active site of PqsE,
198 partially restoring WT activity. Indeed, whereas PqsE(E182W) exhibits reduced binding
199 affinity for the active site fluorescent probe, BB562, PqsE(E182W/E280A) displays WT
200 binding affinity for the probe (Figure 2c). Furthermore, PqsE(E182W) has reduced
201 hydrolytic capacity for a synthetic ester substrate, with only 7% activity relative to WT
202 PqsE. The catalytic function of the PqsE(E182W/E280A) variant was greatly improved by

203 the “unblocking” of the active site (34% compared to WT PqsE, Figure 2d). Consistent
204 with the repositioning of E280 into the PqsE active site contributing to the increased
205 stability of the PqsE(E182W) protein relative to WT PqsE, introduction of the E280A
206 substitution reduced the T_m of the PqsE(E182W/E280A) protein to nearly that of WT PqsE
207 (Figure 2e).

208 Introduction of the E280A alteration into PqsE(E182W) partially corrects the
209 defects in small molecule binding and hydrolysis. Nonetheless, the PqsE(E182W/E280A)
210 variant remains incapable of enhancing RhlR transcription factor activity in an *Escherichia*
211 *coli* reporter assay and it does not drive pyocyanin production in *P. aeruginosa* PA14
212 (Figure 3a and 3b, respectively). Likewise, PqsE(E182W/E280A) is not improved for
213 interaction with RhlR *in vitro* (Figure 4a). These findings further demonstrate the
214 independence of the PqsE catalytic and virulence functions. Curiously, neither the
215 PqsE(E182W) nor the PqsE(E182W/E280A) structure showed any changes in the region
216 of the protein that interacts with RhlR (R243, R246, and R247 on helix 5, Figure 2a and
217 2b, respectively). This result preliminarily suggests that either PqsE possesses an
218 additional region of interaction with RhlR, perhaps employing the G270-L281 loop that is
219 rearranged in PqsE(E182W) or partially disordered in PqsE(E182W/E280A), or
220 alternatively, that a particular conformation of the G270-L281 loop is required to
221 allosterically promote the interaction with RhlR. Irrespective of the underlying mechanism,
222 the above structural and biochemical analyses characterizing PqsE(E182W/E280A) show
223 that it is possible to disrupt the PqsE-RhlR interaction by manipulating the integrity of the
224 G270-L281 loop that forms one face of the PqsE active site.
225

226 *PqsE variants harboring combinations of substitutions decouple catalytic activity from*
227 *RhlR interaction.*

228 Our previous and above work comparing the inhibitor mimetic and RhlR non-
229 interacting PqsE variants to the catalytically inactive PqsE(D73A) protein strongly suggest
230 that the ability of PqsE to interact with RhlR and, in turn, drive virulence phenotypes is
231 independent of PqsE enzyme activity. To confirm this notion, and, additionally, to explore
232 the potential for influence of one activity on the other, we constructed PqsE variants
233 containing combinations of amino acid substitutions underlying defects in enzyme activity,
234 RhlR interaction, or both functions. Purity of these PqsE variant proteins was verified by
235 SDS-PAGE analysis (Figure S2). We assessed the phenotypes of this set of variants *in*
236 *vitro*, in recombinant *E. coli*, and in *P. aeruginosa* PA14. Specifically, we measured
237 interaction of the purified PqsE variant proteins with RhlR by our pull-down assay (Figure
238 4a), intrinsic stability by T_m measurements (differential scanning fluorimetry, DSF),
239 catalytic function by hydrolysis of the synthetic ester substrate 4-methylumbelliferyl
240 butyrate (MU-butyrate), and active site accessibility via binding of the fluorescent active
241 site probe, BB562 (Figure 4b). We measured enhancement of RhlR transcriptional activity
242 in the *E. coli* reporter assay and virulence by pyocyanin production in *P. aeruginosa* PA14
243 (Figure 4b). WT PqsE and the variants PqsE(E280A), PqsE(D73A), PqsE(E182W), and
244 PqsE(NI) have all been previously characterized in this suite of assays and were included
245 in our analyses for comparison to the variants containing combinations of substitutions.
246 As shown in Figure 4 (and Figures S3 and S4), the ability of PqsE to form a complex with
247 RhlR always tracked with activation of RhlR transcription factor activity and pyocyanin

248 production. By contrast, enzymatic capability did not correlate with the ability to form a
249 complex with RhlR, activate RhlR transcription, or to produce pyocyanin.

250 One potential complication in the above analyses is that PqsE proteins harboring
251 the "NI" triple arginine substitutions are less stable than WT and other of our variant PqsE
252 proteins when overproduced in cells from a plasmid. Therefore, all variant proteins
253 containing the NI substitutions were detected at lower levels compared to the other PqsE
254 variant proteins in both *E. coli* and *P. aeruginosa* PA14 cell lysates (Figures S5 and S6).
255 This feature could potentially have been the source of their apparent reduced activities in
256 the RhlR transcriptional reporter assay and the pyocyanin assay. Our results with the
257 PqsE(E182W/NI) variant show, however, that this is not the case. Due to the stabilizing
258 effect of the E182W alteration (Figures 2 and S3), the PqsE(E182W/NI) protein was
259 produced and detected at WT levels in both *E. coli* and *P. aeruginosa* lysates (Figures S5
260 and S6). Nonetheless, PqsE(E182W/NI) was completely inactive in both the pyocyanin
261 production and RhlR transcriptional activity cell-based assays (Figure 3). This result
262 confirms that the inability of select PqsE variants to activate RhlR and drive pyocyanin
263 production stems from loss of the PqsE-RhlR interaction, and is not the result of
264 decreased PqsE protein production or stability.

265

266 *Synthetic optimization of an active site-targeting small molecule scaffold.*

267 The results of our structural and mutagenic analyses suggest that manipulation of
268 the PqsE active site, such that the G270-L281 loop becomes rearranged or disordered
269 will result in decreased *P. aeruginosa* virulence due to inhibition of the PqsE-RhlR
270 interaction. Thus, it is of interest to develop molecules that bind in the PqsE active site

271 and, in so doing, inhibit the PqsE-RhlR interaction. We previously characterized two
272 active site-targeting PqsE inhibitors, BB391 and BB393 (20). Crystallographic analyses
273 of each compound bound to PqsE revealed their respective binding poses and
274 interactions in the active site. Each inhibitor exhibited mid-nanomolar competition with the
275 BB562 active site probe for binding to PqsE (20).

276 Guided by our crystal structures of BB391 and BB393 bound to PqsE, we designed
277 a series of BB391-BB393 hybrid derivatives to probe the contributions of each moiety to
278 binding affinity (Figure 5a). BB580 and BB581 were designed as the core hybrid
279 structures, in which BB580 maintained the same amide bond orientation as in BB391,
280 and BB581 possessed the amide bond orientation of BB393 (see position "1" in Figure
281 5a). BB580 outcompeted the BB562 probe with an EC_{50} of 99 nM compared to BB581
282 which exhibited an EC_{50} of 281 nM (Figure 5b,c). This result demonstrates that
283 preservation of the BB391 amide bond orientation coupled with the indazole ring, also
284 from BB391, is superior for proper positioning of the carbonyl oxygen to form a hydrogen
285 bond with PqsE residue S285. The structure of BB391 bound to PqsE showed that the
286 possibility existed for pi-stacking between the core phenyl ring and the H71 residue.
287 Derivatives BB585, BB586, and BB589 were designed to test enhancement of pi stacking
288 with alternative aromatic groups at this core position (see position "2" in Figure 5a). None
289 of these three derivatives, featuring thiazole, pyrazole, or pyridine rings, respectively,
290 bound as tightly as BB580, and therefore among the molecules tested, a phenyl ring was
291 deemed ideal at this core position (Figure 5b,c). Finally, derivatives BB582, BB583,
292 BB584, BB587, and BB588 were designed to assess the importance of a hydrophobic
293 moiety on the BB393 molecule (see position "3" in Figure 5a), which in the crystal

294 structure, nestles into a hydrophobic groove near the solvent-exposed entrance to the
295 PqsE active site. The results with BB587 and BB588 show that elimination of either the
296 methyl or ethyl groups, respectively, leads to slightly decreased binding affinity (EC_{50} =
297 273 nM and 290 nM, respectively). However, if the morpholine ring is removed and either
298 a phenyl (BB583) or tert-butyl (BB584) group is installed, a modest increase in binding
299 affinity is achieved (EC_{50} = 71 nM and 34 nM, respectively) (Figure 5b,c). Such
300 improvement was not observed for BB582, featuring a pyrazine ring, suggesting that
301 increased hydrophobicity of this portion of the molecule tracks with increased
302 engagement of the hydrophobic groove in PqsE. None of the derivatives described here
303 inhibit the PqsE-RhlR interaction. Within that context, BB584 displayed the tightest
304 binding to PqsE, and provides a starting scaffold for the design of new derivatives.

305 We determined the crystal structure of BB584 bound to PqsE, which showed a
306 similar orientation in the active site and similar ligand-protein interactions to those
307 observed in the crystal structures of PqsE with BB391 and BB393 bound in the active site
308 (Figure 5d). Specifically, the nitrogen on the indazole ring of BB584 bonds with the Fe2
309 atom, displacing a water molecule that normally resides at this position. Two additional
310 hydrogen bonds exist between BB584 and PqsE sidechains: the BB584 amide oxygen
311 with the hydroxyl group of the S285 sidechain, and the BB584 urea oxygen with the
312 backbone amide N-H of residue Y72. As predicted, the tert-butyl group tucks into the
313 hydrophobic groove that sits between the α-helix consisting of PqsE residues S104-L116
314 and the backbone of the conserved ^{69}HXHXDH^{74} motif. Analogous to the structures of
315 BB391 and BB393 bound to PqsE, no significant conformational changes in the protein
316 were induced by binding of BB584 (RMSD of 0.24 Å for 293 Cα atoms), possibly

317 explaining why none of the three compounds disrupt the PqsE-RhlR interaction.
318 Nonetheless, the structures of these ligands bound to WT PqsE along with the structures
319 of PqsE(E182W) and PqsE(E182W/E280A) can be used as guides in the design of new
320 derivatives with the potential to disrupt the interaction between PqsE and RhlR.
321
322 **Discussion**
323
324 PqsE has two activities, a protein-protein interaction with RhlR, which increases
325 RhlR transcriptional activity at target promoters, and an esterase activity, the substrate
326 and product of which are currently unknown. We showed that these two functions are
327 separable. Moreover, we engineered a set of PqsE variant proteins that possess every
328 combination of the two activities (catalytic^{+}/interaction^{+}, catalytic^{-}/interaction^{+},
329 catalytic^{+}/interaction^{-}, and catalytic^{-}/interaction^{-}). Analysis of these proteins, coupled with
330 previous work, shows that the PqsE-RhlR interaction is linked to virulence factor
331 production in *P. aeruginosa* PA14. Here, we demonstrated that the PqsE-RhlR interaction
332 also controls development of *P. aeruginosa* PA14 biofilm morphology and is crucial for
333 establishing an infection in a host animal. Remarkably, PqsE catalytic function is
334 dispensable for regulation of RhlR-transcriptional activity, biofilm morphology, virulence
335 factor production, and animal infectivity. As the PqsE variant phenotypes are consistent
336 between all assays performed, the set of cell-based assays we employ here can
337 effectively be used in lieu of infectivity assays in animals to probe and predict the potential
338 of small molecules as *P. aeruginosa* antibiotics that target PqsE.

339 Our finding that the PqsE-RhlR interaction was disrupted following introduction of
340 the E182W substitution in the PqsE active site was surprising given that this residue is
341 distal to the RhlR interaction site (21). The crystal structure of PqsE(E182W) revealed
342 that a loop rearrangement inserts the E280 residue into the active site to coordinate both
343 of the iron atoms at this site. It is the repositioning of E280 in the PqsE(E182W) variant –
344 blocking substrate access to the catalytic iron atoms – that is responsible for the "inhibitor
345 mimic" nature of this variant. Catalytic activity is restored in the PqsE(E182W/E280A)
346 variant because the alanine substitution clears the active site enabling substrate binding,
347 however, PqsE(E182W/E280A) remains incapable of interacting with RhlR (Figures 3 and
348 4). Analysis of the PqsE(E182W/E280A) structure, and the surprisingly modest
349 conformational changes that are apparent compared to the structures of WT PqsE and
350 PqsE(E182W) (Figure 2a,b), suggest that the structural integrity of the G270-L281 loop
351 is essential for PqsE to interact with RhlR. These results confirm that, although the RhlR-
352 interaction is independent of PqsE catalytic activity, structural changes induced through
353 the active site of PqsE can disrupt interaction with RhlR.

354 All prior crystal structures of WT PqsE showed that the E280 residue resides on
355 the surface with the glutamate sidechain directed outward into the solvent. Our data show
356 that single substitution of this glutamate with alanine (i.e., PqsE(E280A)) increased
357 accessibility of the PqsE active site (Figure 2c). This finding potentially points to naturally
358 occurring PqsE conformational dynamics in which the position of the E280 sidechain
359 alternates between facing the solvent and being inserted into the active site. While not
360 proven, it is possible that E280 serves as a dynamic gate-keeper residue for the active
361 site. Perhaps, its position determines whether PqsE will undergo catalysis and/or will

362 interact with RhlR. Such a mechanism would make considerations of the PqsE E280
363 sidechain position key for future drug discovery efforts (26).
364 Figure 5 presents a new series of molecules, inspired by the previous PqsE
365 inhibitors BB391 and BB393, all of which bind in the PqsE active site. Our competitive
366 binding assay allowed us to rank derivatives by their relative affinities providing
367 preliminary structure-activity relationships. Among this set, compound BB584 binds most
368 tightly in the PqsE active site (EC_{50} = 34 nM). The crystal structure of the PqsE-BB584
369 complex solved here (Figure 5c) provides needed information for launching structure-
370 guided design of the next generation of molecules targeting the PqsE active site. None of
371 the inhibitors characterized here perturb the PqsE-RhlR interaction. However, our PqsE
372 variant analysis and companion structures make it clear that it should be possible to
373 design high affinity active site-targeting compounds that disrupt the PqsE-RhlR interaction
374 via an allosteric mechanism, presumably involving movement of the G270-L281 loop.
375
376 **Methods**
377
378 *Strains, Media, and Molecular Procedures*
379 The *P. aeruginosa* UCBPP-PA14 strain was used as the parental strain for all
380 experiments involving *P. aeruginosa*. All strains were grown in Luria-Bertani broth, unless
381 otherwise stated, and antibiotics were used at the following concentrations: ampicillin
382 (200 µg/mL), kanamycin (100 µg/mL), tetracycline (10 µg/mL), carbenicillin (400 µg/mL),
383 gentamycin (30 µg/mL), and irgasan (100 µg/mL). Plasmids were constructed following a
384 previously reported site-directed mutagenesis protocol (27) and were transformed into *P.*

385 *aeruginosa* PA14 strains as described (28). Deletion of and point mutations in *pqsE* were
386 generated by a previously reported method, with some modifications (24). Briefly, *pqsE*
387 variants were cloned onto the pEXG2 vector. *E. coli* SM10λ*pir* carrying each pEXG2-
388 *pqsE*-containing plasmid was mated with *P. aeruginosa* PA14 or the Δ*rhlI* strain and
389 exconjugants were selected on LB agar containing gentamycin and irgasan. Colonies
390 were grown in LB medium at 37 ˚C for 1-2 h and plated on LB agar containing 5% sucrose
391 to force elimination of the *sacB* gene on the plasmid. Resulting colonies were patched
392 onto LB agar plates and onto plates containing gentamycin, and *pqsE* variants in $Gent^S$
393 colonies were confirmed by sequencing. Strains used in this study are listed in
394 Supplemental Table S1.
395
396 *General Methods*
397 6xHis-PqsE proteins were purified for biochemical assays (tagged) and crystallography
398 (tag removed) as described previously (20). Enzyme activities of purified 6xHis-PqsE
399 variants were measured as previously reported with 4-methylumbelliferyl butyrate (MU-
400 butyrate) as the substrate (21). Fluorescence polarization assays with the BB562 active
401 site probe were performed as described (20). The melting temperature (T_m) of each
402 purified 6xHis-PqsE variant was measured using differential scanning fluorimetry (DSF)
403 as described previously (20). Interaction between PqsE and RhlR proteins *in vitro* was
404 measured as described previously using pull-down assays (20). Pyocyanin production by
405 *P. aeruginosa* PA14 strains carrying *pqsE* variants on the pUCP18 plasmid was
406 measured as described (20). The ability of PqsE variants to increase RhlR transcription
407 factor activity in an *E. coli* reporter assay was assessed as previously described (20). All

408 small molecule syntheses and characterization are described in the Supplementary
409 Information.
410
411 *Colony Biofilm Morphology Assay*
412 Cultures were grown overnight in LB broth with shaking at 37 ˚C and 1 µL of culture was
413 spotted onto a 60 x 15 mm Petri plate containing 10 mL biofilm medium (1% Tryptone,
414 1% agar, 40 mg/L Congo Red, 20 mg/L Coomassie Brilliant Blue). Biofilms were grown
415 at 25 ˚C for several days and imaged throughout their development on a Leica
416 stereomicroscope M125 mounted with a Leica MC170 HD camera at 7.78x magnification.
417
418 *Mouse Lung Infection Studies*
419 For all mouse experiments, *P. aeruginosa* strains were grown on *Pseudomonas* Isolation
420 Agar (PIA) for 16–18 h at 37°C and suspended in PBS to an OD_{600} of 0.5, corresponding
421 to ~10^9 CFU/mL. These samples were adjusted spectrophotometrically and then diluted
422 to the appropriate OD_{600} in phosphate-buffered saline (PBS). Eight-to-ten-week-old
423 female BALB/c mice (Jackson Laboratories, Bar Harbor, ME) were anesthetized by
424 intraperitoneal (i.p.) injection of 0.2 mL of a mixture of ketamine (25 mg/mL) and xylazine
425 (12 mg/mL). Mice were infected by noninvasive intratracheal instillation (29) of 50 µL of
426 ~3×10^6 CFU of *P. aeruginosa* WT or isogenic mutants. Mice were euthanized at 24 and
427 48 h post-infection and whole lungs were collected aseptically, weighed, and
428 homogenized in 1 mL of PBS. Bacterial loads in tissue homogenates were enumerated
429 by serial dilution and plating on PIA. Comparison and analyses of the numbers of viable
430 bacteria obtained in lung homogenates were performed using GraphPad Prism version 7

431 software. Results were analyzed using one-way analysis of variance (ANOVA) and were
432 compared using the Kruskal-Wallis test for comparison of three groups or the Mann-
433 Whitney *U* test for analysis of two groups.
434
435 *Protein Crystallography*
436 Purified proteins (~10 mg/mL) and protein-compound complexes were crystallized by
437 hanging drop vapor diffusion at 22 ˚C following mixing at a 1:1 ratio with well buffer.
438 Crystallization buffers used were as follows: PqsE(E182W) (0.1 M HEPES pH 7.5, 0.2 M
439 $MgCl_2$, 15% (w/v) PEG 400) cryoprotected with 20% (v/v) glycerol prior to freezing,
440 PqsE(E182W/E280A) (0.1 M HEPES pH 7.5, 0.2 M $MgCl_2$, 27% (w/v) PEG 400)
441 cryoprotected with 10% (v/v) ethylene glycol prior to freezing, and PqsE-BB584 (0.1 M
442 HEPES pH 7.5, 0.2 M $MgCl_2$, 15% (v/v) 2-propanol) cryoprotected with 30% (v/v) ethylene
443 glycol with additional BB584 (50 μM) in the cryoprotectant solution. Crystals typically
444 formed within 48 h, but in some cases, took up to 5 days to form. PqsE(E182W),
445 PqsE(E182W/E280A), and PqsE-BB584 crystals each grew in the same trigonal space
446 group as had been previously observed for WT PqsE, PqsE-BB391 and PqsE-BB393
447 ($P3_221$, a=b= 60 Å c= 146 Å $\alpha=\beta=90^o$, $\gamma=120^o$) with one molecule in the asymmetric unit.
448 Data were collected on either the 17-ID-1 beamline of the NSLS-II synchrotron
449 (PqsE(E182W) and PqsE(E182W/E280A)), or on a Rigaku MicroMax 007HF rotating
450 anode source (PqsE-BB584) (Table S2). Data were processed either with XDS (30) and
451 AIMLESS (31) or with DENZO and SCALEPACK (32). The starting model for each
452 refinement was a prior ligand-bound structure (7KGX, (20)) with the ligand and water
453 molecules removed but the iron atoms retained, subjected to rigid-body refinement

454 followed by conventional refinement using Phenix.refine (33). The structures were
455 iteratively rebuilt using Coot (34) and refined with Phenix.refine. Both PqsE variant
456 proteins exhibited significant conformational changes in a loop region (G270-L281)
457 relative to the starting model, which remodeled the active site. In the case of the BB584
458 ligand, an atomic model of the ligand was fit to the difference electron density observed
459 in the active site of PqsE and refined with partial occupancy (0.93). Final refinement
460 statistics are shown in Table S2 including the identifiers for the structures' depositions in
461 the Protein Data Bank (PqsE(E182W) PDB ID: 7TZ9, PqsE(E182W/E280A): 7U6G, and
462 PqsE-BB584 PDB ID: 7TZA).
463
464 **Ethics Statement**
465
466 All mouse procedures were performed in accordance with the established guidelines of
467 the Emory University Institutional Animal Care and Use Committee (IACUC) under
468 protocol number DAR-201700441. This study was carried out in strict accordance with
469 established guidelines and policies at Emory University School of Medicine, the
470 recommendations in the Guide for Care and Use of Laboratory Animals (35), as well as
471 local, state, and federal laws.
472
473 **Acknowledgements**
474
475 We thank members of the Bassler laboratory for helpful advice and discussions. We are
476 grateful to William Miller and Brad Henke for guidance in chemical strategies and

477 synthetic procedures. Molecules used in this study were synthesized at WuXi AppTec.
478 Protein crystallography was performed in the Macromolecular Crystallography Core
479 Facility at Princeton University. The AMX beamline of the National Synchrotron Light
480 Source II, a U.S. Department of Energy (DOE) Office of Science User Facility operated
481 for the DOE Office of Science by Brookhaven National Laboratory was also used under
482 Contract DE-SC0012704. This work was supported by the Howard Hughes Medical
483 Institute, NIH grant 2R37GM065859, and National Science Foundation grant MCB-
484 2043238 to B.L.B., and NIH grant F32GM134583 to I.R.T. The content herein is solely
485 the responsibility of the authors and does not represent the official views of the National
486 Institutes of Health. The authors declare that they have no competing financial interests.
487

488 **Author Contributions**

489

490 I.R.T, P.D.J., and D.A.M. conducted experiments; I.R.T, P.D.J., D.A.M., J.B.G., and
491 B.L.B. designed experiments and prepared the manuscript.

492

493 **Figure Legends**

494

495 **Figure 1: PqsE variants that are deficient in interaction with RhlR display**
496 **attenuated pathogenicity.** a) The Rhl QS system in *P. aeruginosa*. See text for details.
497 b) Pyocyanin production by *P. aeruginosa* PA14 harboring the designated *pqsE* alleles at
498 the native *pqsE* locus. The WT PA14 pyocyanin production level was set to 100%. Results
499 are the average of two biological replicates. Error bars represent standard deviations. c)

500 Colony biofilm morphologies of the designated *P. aeruginosa* PA14 strains. Biofilms were
501 imaged after 5 d of growth at 7.78x magnification. Images are representative of three
502 biological replicates. d) Lung colonization by the designated *P. aeruginosa* PA14, Δ*pqsE*,
503 *pqsE(D73A)*, *pqsE(E182W)*, or the *pqsE(NI)* strains in the murine infection model. Mice
504 were euthanized at 24 and 48 h post-infection, and lung tissues were processed as
505 described in Methods. All samples were plated for viable CFU on PIA. Each symbol
506 represents the value for a single mouse. The data are pooled from two independent
507 experiments. Error bars represent SEM. Statistical differences were determined using
508 one-way ANOVA test and are as follows: ***, $P < 0.001$; *, $P < 0.05$; NS means not
509 significant.
510
511 **Figure 2: The PqsE E182W substitution induces a loop rearrangement that**
512 **repositions residue E280.** a) Structure of PqsE(E182W) (blue) overlaid with that of WT
513 PqsE (PDB: 2Q0I, gray). The active site iron atoms are in shown in orange. The red arrow
514 indicates repositioning of E280 in PqsE(E182W) relative to its position in WT PqsE. b)
515 Structure of PqsE(E182W/E280A) (maroon) overlaid with that of WT PqsE (as in a). In
516 panels a and b, residue E280 is shown in stick representation. c) Binding of WT and
517 variant PqsE proteins to the active site fluorescent probe BB562. K_{app} was determined in
518 two independent experiments performed in triplicate. d) Hydrolysis of 4-methylumbelliferyl
519 butyrate by the designated purified PqsE proteins. Values are represented as % activity
520 of WT PqsE protein. Results are the average of two independent experiments performed
521 in triplicate. Error bars represent standard deviations. e) First derivative plots (dF/dT is
522 defined as the change in SYPRO Orange fluorescence divided by change in temperature)

523 of melting curves for the designated PqsE proteins. The peak of each curve is defined as
524 the T_m of that protein.
525
526 **Figure 3: The PqsE E280A substitution does not restore activation of RhlR**
527 **transcriptional activity or pyocyanin production.** a) Light production from *E. coli*
528 carrying P_{BAD}-*rhlR*, P*rhlA-luxCDABE*, and the designated *pqsE* allele on the pACYC184
529 plasmid was measured following growth in the presence of 100 nM C4-HSL. The "-"
530 symbol represents the strain carrying the empty pACYC184 vector. Results are the
531 average of two biological replicates performed in technical triplicate. b) Pyocyanin
532 production was measured from Δ*pqsE P. aeruginosa* PA14 carrying the designated *pqsE*
533 allele on the pUCP18 plasmid. The "-" symbol represents the strain carrying an empty
534 pUCP18 plasmid. Results shown are the average of two biological replicates. Pyocyanin
535 production from the strain with WT PqsE was set to 100%. Error bars represent standard
536 deviations.
537
538 **Figure 4: PqsE enzymatic activity is dispensable for RhlR interaction, RhlR**
539 **transcriptional activity, and pyocyanin production.** a) SDS-PAGE analysis of protein
540 complexes formed in *in vitro* pull-down assays. 6xHis-PqsE proteins were immobilized on
541 Ni resin and exposed to lysate containing RhlR. The resulting protein complexes were
542 washed and eluted from the Ni resin and loaded into the lanes of the gel. PqsE appears
543 as a ~34 kDa band and RhlR as a ~28 kDa band. For the variant combinations, "X"
544 denotes that the protein in that lane contains the designated substitutions listed to the
545 right. b) Measured activities of PqsE variants in the designated assays. The full data from

546 these analyses are provided in Figures S3 and S4 including replicate and statistical
547 information. “ND” denotes that error could not be calculated for the binding curve, which
548 occurred when the binding curve was too shallow or did not achieve saturation.
549
550 **Figure 5: Optimization of new PqsE active site-targeting small molecules.** a)
551 Structures of the precursor molecules BB391 and BB393 and the hybrid derivative
552 BB580. Positions denoted 1, 2, and 3 were derivatized to explore binding affinity for the
553 PqsE active site. b) Fluorescence polarization competition curves for select BB391-
554 BB393 hybrid derivatives competing with the BB562 active site probe for binding to PqsE.
555 Polarization value for PqsE-BB562 in the absence of competitor is defined as 100% Probe
556 Bound. All polarization values were background-subtracted by the reading for the probe
557 in the absence of PqsE (background fluorescence). c) Competitive fluorescence
558 polarization EC_{50} values calculated for all BB391-BB393 derivatives, determined from one
559 experiment performed in triplicate. d) Structure of BB584 bound to PqsE. Both the BB584
560 molecule and key PqsE amino acid sidechains are shown as sticks. Amino acid sidechain
561 carbons are depicted in gray and BB584 carbons are shown in tan. Iron atoms and water
562 molecules are shown as orange and green spheres, respectively. Oxygen and nitrogen
563 atoms are in red and blue, respectively. Hydrogen bonds are shown as dotted yellow
564 lines.
565
566 **References**
567
568 1. Driscoll JA, Brody SL, Kollef MH. The epidemiology, pathogenesis and treatment of
569 Pseudomonas aeruginosa infections. Drugs. 2007;67(3):351–68.

570 2. Kang CI, Kim SH, Kim HB, Park SW, Choe YJ, Oh MD, et al. Pseudomonas
571 aeruginosa bacteremia: risk factors for mortality and influence of delayed receipt of

572 effective antimicrobial therapy on clinical outcome. Clin Infect Dis. 2003 Sep
573 15;37(6):745–51.

574 3. Breidenstein EBM, de la Fuente-Núñez C, Hancock REW. Pseudomonas
575 aeruginosa: all roads lead to resistance. Trends Microbiol. 2011 Aug;19(8):419–26.

576 4. De Oliveira DMP, Forde BM, Kidd TJ, Harris PNA, Schembri MA, Beatson SA, et al.
577 Antimicrobial Resistance in ESKAPE Pathogens. Clin Microbiol Rev. 2020 Jun
578 17;33(3).

579 5. Moradali MF, Ghods S, Rehm BHA. Pseudomonas aeruginosa Lifestyle: A Paradigm
580 for Adaptation, Survival, and Persistence. Frontiers in Cellular and Infection
581 Microbiology [Internet]. 2017;7. Available from:
582 https://www.frontiersin.org/article/10.3389/fcimb.2017.00039

583 6. Chadha J, Harjai K, Chhibber S. Revisiting the virulence hallmarks of Pseudomonas
584 aeruginosa: a chronicle through the perspective of quorum sensing. Environ
585 Microbiol. 2021 Sep 24;

586 7. O'Loughlin CT, Miller LC, Siryaporn A, Drescher K, Semmelhack MF, Bassler BL. A
587 quorum-sensing inhibitor blocks Pseudomonas aeruginosa virulence and biofilm
588 formation. Proc Natl Acad Sci U S A. 2013 Oct 29;110(44):17981–6.

589 8. Rutherford ST, Bassler BL. Bacterial quorum sensing: its role in virulence and
590 possibilities for its control. Cold Spring Harb Perspect Med. 2012 Nov 1;2(11).

591 9. Passador L, Cook JM, Gambello MJ, Rust L, Iglewski BH. Expression of
592 Pseudomonas aeruginosa virulence genes requires cell-to-cell communication.
593 Science. 1993 May 21;260(5111):1127–30.

594 10. Heeb S, Fletcher MP, Chhabra SR, Diggle SP, Williams P, Cámara M. Quinolones:
595 from antibiotics to autoinducers. FEMS Microbiology Reviews. 2011;35(2):247–74.

596 11. Pesci EC, Milbank JB, Pearson JP, McKnight S, Kende AS, Greenberg EP, et al.
597 Quinolone signaling in the cell-to-cell communication system of Pseudomonas
598 aeruginosa. Proc Natl Acad Sci U S A. 1999 Sep 28;96(20):11229–34.

599 12. Pearson JP, Gray KM, Passador L, Tucker KD, Eberhard A, Iglewski BH, et al.
600 Structure of the autoinducer required for expression of Pseudomonas aeruginosa
601 virulence genes. Proc Natl Acad Sci U S A. 1994 Jan 4;91(1):197–201.

602 13. Pearson JP, Passador L, Iglewski BH, Greenberg EP. A second N-acylhomoserine
603 lactone signal produced by Pseudomonas aeruginosa. Proc Natl Acad Sci USA.
604 1995 Feb 28;92(5):1490–4.

605 14. Rampioni G, Falcone M, Heeb S, Frangipani E, Fletcher MP, Dubern JF, et al.
606 Unravelling the Genome-Wide Contributions of Specific 2-Alkyl-4-Quinolones and

607 PqsE to Quorum Sensing in Pseudomonas aeruginosa. PLOS Pathogens. 2016 Nov
608 16;12(11):e1006029.

609 15. Drees SL, Fetzner S. PqsE of Pseudomonas aeruginosa Acts as Pathway-Specific
610 Thioesterase in the Biosynthesis of Alkylquinolone Signaling Molecules. Chem Biol.
611 2015 May 21;22(5):611–8.

612 16. Lee J, Zhang L. The hierarchy quorum sensing network in Pseudomonas
613 aeruginosa. Protein Cell. 2015 Jan;6(1):26–41.

614 17. Farrow JM, Sund ZM, Ellison ML, Wade DS, Coleman JP, Pesci EC. PqsE functions
615 independently of PqsR-Pseudomonas quinolone signal and enhances the rhl
616 quorum-sensing system. J Bacteriol. 2008 Nov;190(21):7043–51.

617 18. Groleau MC, de Oliveira Pereira T, Dekimpe V, Déziel E. PqsE Is Essential for RhlR-
618 Dependent Quorum Sensing Regulation in Pseudomonas aeruginosa. mSystems.
619 2020 May 26;5(3).

620 19. Zender M, Witzgall F, Drees SL, Weidel E, Maurer CK, Fetzner S, et al. Dissecting
621 the Multiple Roles of PqsE in Pseudomonas aeruginosa Virulence by Discovery of
622 Small Tool Compounds. ACS Chem Biol. 2016 17;11(6):1755–63.

623 20. Taylor IR, Paczkowski JE, Jeffrey PD, Henke BR, Smith CD, Bassler BL. Inhibitor
624 Mimetic Mutations in the Pseudomonas aeruginosa PqsE Enzyme Reveal a Protein-
625 Protein Interaction with the Quorum-Sensing Receptor RhlR That Is Vital for
626 Virulence Factor Production. ACS Chem Biol. 2021 Apr 16;16(4):740–52.

627 21. Simanek KA, Taylor IR, Richael EK, Lasek-Nesselquist E, Bassler BL, Paczkowski
628 JE. The PqsE-RhlR Interaction Regulates RhlR DNA Binding to Control Virulence
629 Factor Production in Pseudomonas aeruginosa. Microbiol Spectr. 2022 Jan
630 12;10(1):e0210821.

631 22. Cesa LC, Mapp AK, Gestwicki JE. Direct and Propagated Effects of Small Molecules
632 on Protein-Protein Interaction Networks. Front Bioeng Biotechnol. 2015;3:119.

633 23. Ran X, Gestwicki JE. Inhibitors of protein-protein interactions (PPIs): an analysis of
634 scaffold choices and buried surface area. Curr Opin Chem Biol. 2018 Jun;44:75–86.

635 24. Mukherjee S, Moustafa D, Smith CD, Goldberg JB, Bassler BL. The RhlR quorum-
636 sensing receptor controls Pseudomonas aeruginosa pathogenesis and biofilm
637 development independently of its canonical homoserine lactone autoinducer. PLOS
638 Pathogens. 2017 Jul 17;13(7):e1006504.

639 25. Mukherjee S, Moustafa DA, Stergioula V, Smith CD, Goldberg JB, Bassler BL. The
640 PqsE and RhlR proteins are an autoinducer synthase–receptor pair that control
641 virulence and biofilm development in Pseudomonas aeruginosa. PNAS. 2018 Sep
642 17;201814023.

643 26. Pricer R, Gestwicki JE, Mapp AK. From Fuzzy to Function: The New Frontier of
644 Protein-Protein Interactions. Acc Chem Res. 2017 Mar 21;50(3):584–9.

645 27. McCready AR, Paczkowski JE, Henke BR, Bassler BL. Structural determinants
646 driving homoserine lactone ligand selection in the *Pseudomonas aeruginosa* LasR
647 quorum-sensing receptor. Proc Natl Acad Sci USA. 2019 Jan 2;116(1):245.

648 28. Choi KH, Kumar A, Schweizer HP. A 10-min method for preparation of highly
649 electrocompetent Pseudomonas aeruginosa cells: Application for DNA fragment
650 transfer between chromosomes and plasmid transformation. Journal of
651 Microbiological Methods. 2006 Mar 1;64(3):391–7.

652 29. Revelli DA, Boylan JA, Gherardini FC. A non-invasive intratracheal inoculation
653 method for the study of pulmonary melioidosis. Front Cell Infect Microbiol.
654 2012;2:164.

655 30. Kabsch W. XDS. Acta Crystallogr D Biol Crystallogr. 2010 Feb;66(Pt 2):125–32.

656 31. Evans PR, Murshudov GN. How good are my data and what is the resolution? Acta
657 Crystallogr D Biol Crystallogr. 2013 Jul;69(Pt 7):1204–14.

658 32. Otwinowski Z, Minor W. Denzo and Scalepack. In: International Tables for
659 Crystallography. 2001. p. 226–35.

660 33. Liebschner D, Afonine PV, Baker ML, Bunkóczi G, Chen VB, Croll TI, et al.
661 Macromolecular structure determination using X-rays, neutrons and electrons:
662 recent developments in Phenix. Acta Crystallogr D Struct Biol. 2019 Oct 1;75(Pt
663 10):861–77.

664 34. Emsley P, Lohkamp B, Scott WG, Cowtan K. Features and development of Coot.
665 Acta Crystallogr D Biol Crystallogr. 2010 Apr;66(Pt 4):486–501.

666 35. Guide for the Care and Use of Laboratory Animals. 8th ed. Washington (DC):
667 National Academies Press (US); 2011.

668
669

670 **Figure 1**

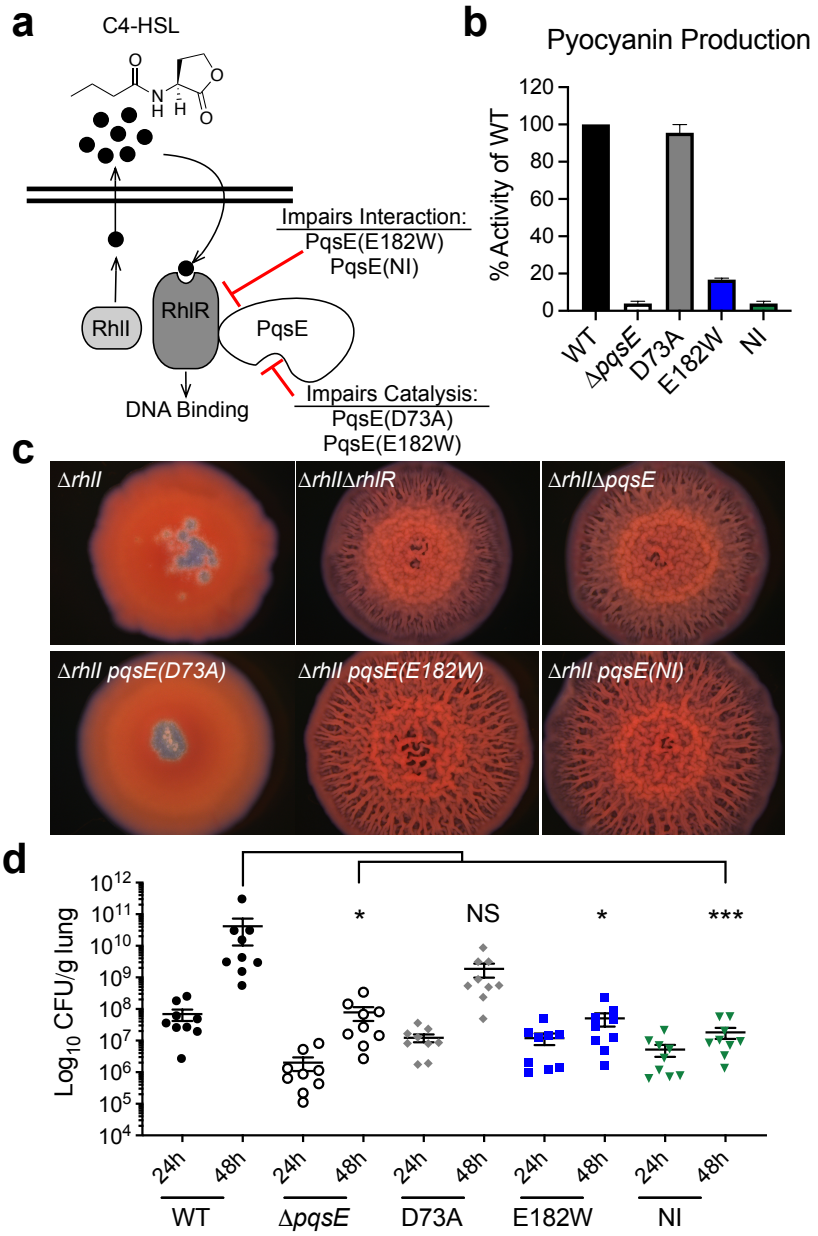

671
672

673 **Figure 2**

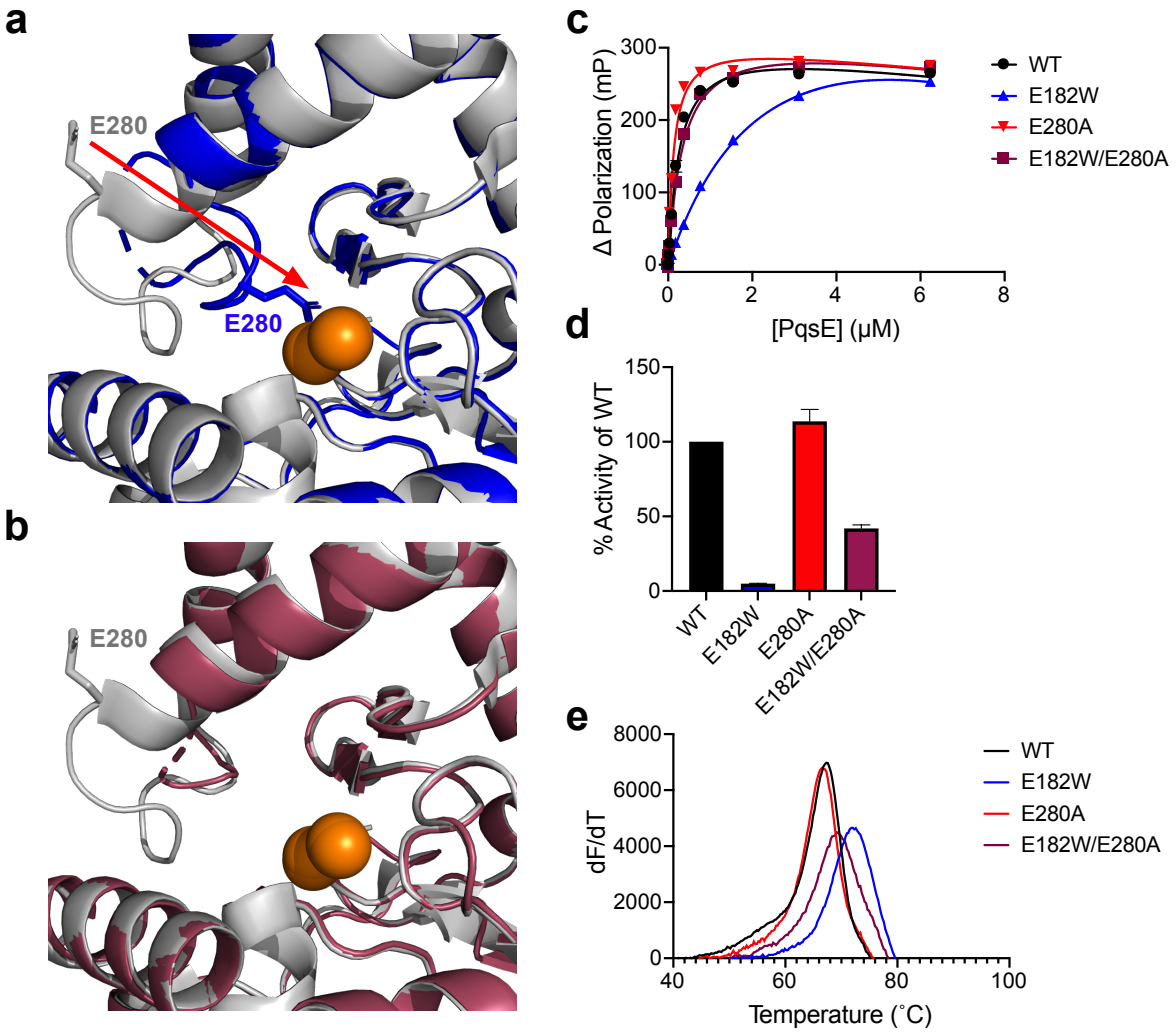

674
675

676 **Figure 3**

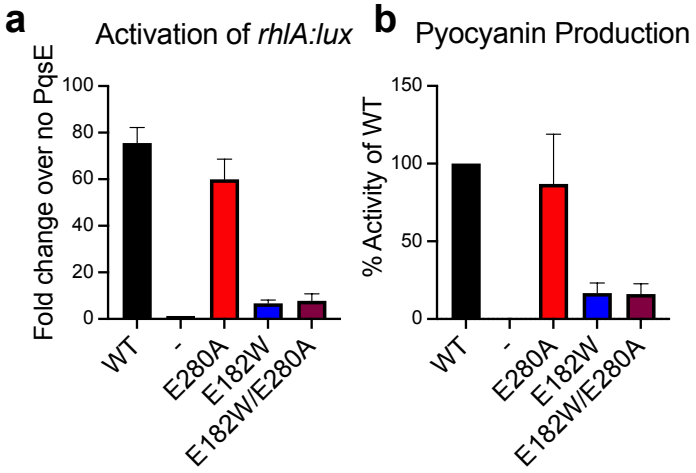

677
678

679
680 **Figure 4**

a

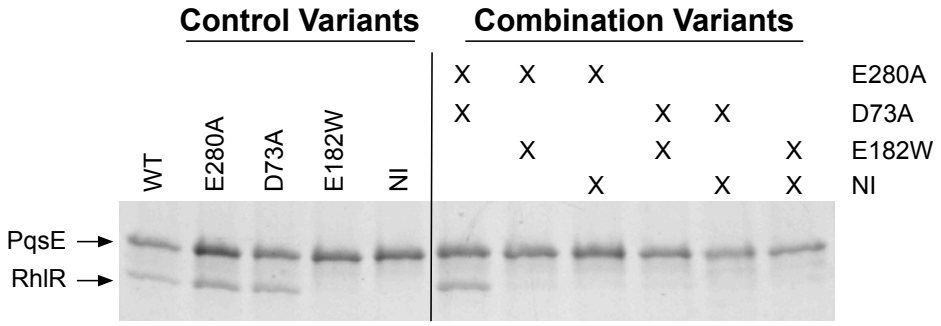

b

PqsE Variant	T_m (˚C)	Hydrolysis (%WT)	BB562 Binding K_{app} (nM)	RhlR Activity (Fold x no PqsE)	Pyocyanin (%WT)
WT	67.3	100	416 ± 170	76 ± 7	100
E280A	66.8	101 ± 3.0	210 ± 90	60 ± 9	87 ± 32
D73A	66.5	0 ± 1.3	507 ± 380	40 ± 6	83 ± 11
E182W	72.1	7 ± 0.0	5730 ± 4000	7 ± 1	17 ± 7
NI	62.8	46 ± 4.5	428 ± 100	1 ± 0	1 ± 1
D73A/E280A	66.3	0 ± 1.2	468 ± 300	22 ± 5	60 ± 20
E182W/E280A	69.4	34 ± 0.7	418 ± 160	8 ± 3	16 ± 7
NI/E280A	61.5	18 ± 0.8	669 ± 220	1 ± 0	2 ± 1
D73A/E182W	68.9	1 ± 0.0	8120 ± ND	6 ± 0	16 ± 6
D73A/NI	61.8	0 ± 0.8	564 ± ND	1 ± 0	1 ± 1
E182W/NI	69.2	0 ± 0.6	4330 ± ND	1 ± 0	1 ± 1

681
682

683 **Figure 5**

a

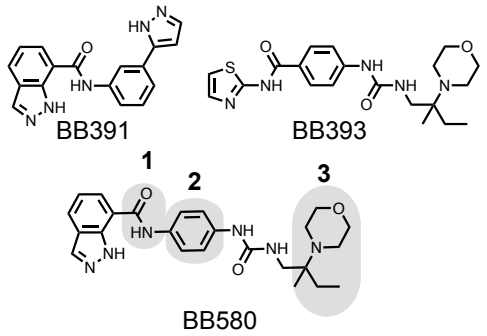

b

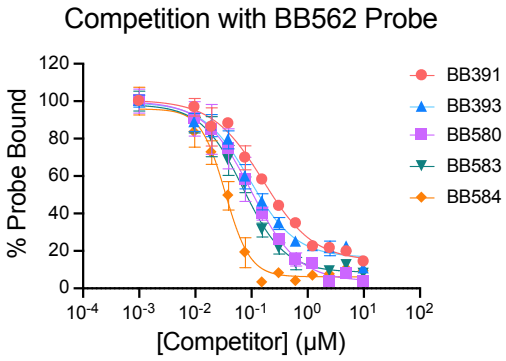

d

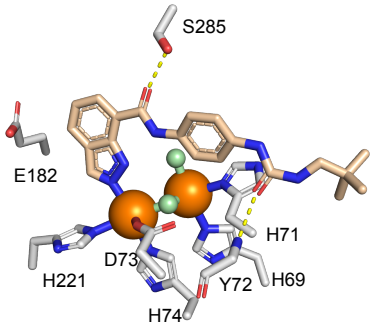

c

Compound	1	2	3	EC_{50} (nM)
BB391				160 ± 54
BB393				93 ± 29
BB580		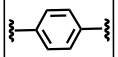	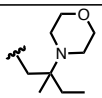	99 ± 44
BB581		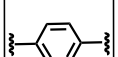	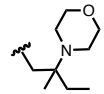	281 ± 331
BB582		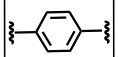		302 ± 141
BB583		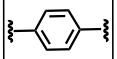		71 ± 43
BB584		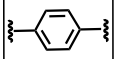		34 ± 15
BB585		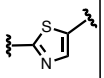		>1,000
BB586		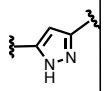		>1,000
BB587		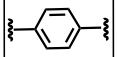		273 ± 85
BB588		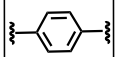		290 ± 106
BB589		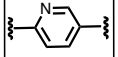		608 ± 647

684